Proceedings of the ASME 2020
International Design Engineering Technical Conferences
and Computers and Information in Engineering Conference
IDETC/CIE2020
August 17-19, 2020, Virtual, Online

DETC2020-22392

A HETEROGENEOUS MODEL FOR GAIT ANALYSIS OF THE LOWER-LIMB AND THE PROSTHESIS COUPLED SYSTEM

Yang Lv[1], Hongbin Fang[2,3,4], Jian Xu[2,3,4], Qining Wang[5], Xiaoxu Zhang[2,3,4*]

[1] Department of Aeronautics and Astronautics, Fudan University, Shanghai 200433, China
[2] Institute of AI and Robotics, Fudan University, Shanghai 200433, China
[3] Shanghai Engineering Research Center of AI & Robotics, Shanghai 200433, China
[4] Engineering Research Center of AI & Robotics, Ministry of Education, Shanghai 200433, China
[5] College of Engineering, Peking University, Beijing 100871, China

ABSTRACT

By considering the coupling effect between the healthy lower-limb and the passive prosthesis, this paper builds a heterogeneous dynamic model for gait analysis, where the motions of the healthy limb and the prosthesis are driven by the central pattern generator (CPG) and the hip joint swing, respectively. The foot-ground contact is modelled as the process of unilateral force reaction rather than the constraint to get a refined representation of the gait motion. The response of the heterogeneous model, solved by numerical calculation, is then analyzed by comparison with a real gait test. Preliminary results show that the heterogeneous model not only describes the amputee's gait well but also reveals a new gait feature of period-doubling. Parameter analysis further indicates that the period-doubling gait will return to the single-period pattern by amplifying the vertical motion of the hip joint at the amputated side. This dynamic bifurcation, which mimics the process of hip swing adaption, provides new insight into the compensatory mechanism for lamely walking.

Keywords: passive prosthesis, central pattern generator, foot-ground contact, dynamic modelling, compensatory mechanism

1. INTRODUCTION

Lower limb prosthesis provides trustworthy support to amputees in normal walking. Its compliance with the motion of the stump and the reaction of the road determine the amputee's experience of wearing comfort. Therefore, the optimization of the prosthesis has attracted much concern from researchers.

Performance optimization of the prosthesis needs a prior refined model, which consists of the boundary representation of foot-ground contact and the motion representations of the prosthesis and the healthy limb.

Current studies [1-3] assume that the foot-ground contact is an ideal constraint. This assumption simplifies the modelling of the system because the reaction force of the contact can be directly represented by the Lagrange equations. However, a refined model should represent the feature of energy dissipation, e.g. the incomplete elastic impact and the friction, during foot-ground contact. The incomplete elastic impact is usually described by the Hunt-Crossley model [4], the Gonthier model [5], and the Kelvin-Voigt model [6], where the last one represents the effect of impact best. More representations, e.g. the Coulomb model [7], the Stribeck model [8, 9], and the LuGre model [10-12], are qualified to describe the friction. Although the latter two models reveal the feature of pre-sliding, a more sophisticated phenomenon in tribology, experiments [13-15] show that the Coulomb model is accurate enough for friction description if the amplitude of motion is of millimeters or above. Taking the fact that the amplitude of one walking step is 0.8 m around, it is reasonable to choose the Coulomb model to describe the friction in foot-ground contact.

The prosthesis and the healthy limb are usually simplified as multibody systems and, consequently, their motions are described by the Lagrange equations of the first kind [3, 16]. The difference between them mainly stays in the form of the driven force.

Clear evidence [17] has shown that the gait of humans is driven by the spinal central pattern generator (CPG), which generates the bioelectric signal with a certain period to stimulate relevant muscles on lower limbs. The model of the CPG usually consists of a group of coupled oscillators that generate limit-

* Contact Author: zhangxiaoxu@fudan.edu.cn (Xiaoxu Zhang)

cycle signals, e.g. the Hopf oscillation [18] and the Matsuoka oscillation [19]. Since the CPG comprehensively combines the rules that govern the biological pattern and mechanical motion, it has also been widely employed to generate either joint trajectories [18, 20] or joint torques [3, 19, 21] to control the gait of bipedal walking robots.

The driving force of the prosthesis can be either passive or active. This paper focuses on the passive kind because it is more economical and reliable. In the passive prosthesis, the driving force only comes from the motion of the hip-joint swing. The hydraulic cylinder, embedded in the prosthetic knee joint, provides the damping force and the restoring force to coordinate the swing of the prosthesis. Noting that the instant center of rotation (ICR) of a human's knee joint moves as a J-shaped trajectory, which provides higher stability during stance and a better smartness during the swing, extensive studies put their emphasis on passive prostheses with the four-bar linkage prosthetic knee [22-24]. These studies treat the motion of the hip joint swing and the foot-ground contact as ideal boundary conditions so that the prosthesis can be modelled independently. However, the reaction force of the prosthesis should affect the hip joint as well as the healthy limb. It will cause a consequent change in the gait. In other words, the prosthesis couples with the healthy limb. Considering that the forms of corresponding driving forces are different, a heterogeneous model should then be built.

Motivated by this need, the present paper reconsiders all factors that participate in the dynamics of the lower-limb system. The Kelvin-Voigt model and the Coulomb model are adopted to simulate the incomplete elastic impact and friction in the foot-ground contact. The CPG based control is employed to mimic the driven force of the healthy limb. The motion representations of the prosthesis and the healthy limb are then integrated based on motion coordination. The response of the heterogeneous model, solved by numerical calculation, is then analyzed by comparison with a real gait test. Preliminary results show that the heterogeneous model not only describes the amputee's gait well but also reveals a new gait feature of period-doubling. Parameter analysis further indicates that the period-doubling gait will return to the single-period pattern by amplifying the vertical motion of the hip joint at the amputated side. This dynamic bifurcation, which mimics the process of hip swing adaption, provides new insight into the compensatory mechanism for lamely walking.

The rest of the paper is organized as follows: Section 2 first introduces the models of the foot-ground contact, the passive prosthesis, and the healthy limb, and then builds the heterogeneous model by coupling the prosthesis and the healthy limb via the hip joint connection. Section 3 gives some preliminary analysis on the motion of the heterogeneous model, where a new insight into the compensatory mechanism for lamely walking is provided. Finally, a summary concludes the paper.

2. MODELLING OF THE HETEROGENEOUS SYSTEM

This paper simplifies the motions of the healthy limb and the prosthesis to be planar. The trunk, the thighs, the shanks, and the feet are all simplified as rigid rods. The schematic view of the coupled systems is given in FIGURE 1, where α_1 and α_2 indicate the swing angles of the thighs, α_{11} and α_{22} represent the swing angles of the healthy and the prosthetic shanks, β_1 and β_2 denote the rotation angles of the feet, θ_A and θ_B indicate the rotation angles of the linkages BC and AD. The trunk stays vertical. x and y are the horizontal and the vertical positions of the hip joint. The prosthesis connects with the stump rigidly by the socket. The angle between the socket and the linkage AB, defined as γ_1, is 90º. The angle between the prosthetic shank and the linkage CD, defined as γ_2, is 24º. The lengths of the healthy limb's thigh, shank and foot are l_{t1}, l_{s1} and l_{f1}, respectively. The ratio of the distance between the heel and the ankle to the whole foot length is r_{f1}. And those of the prosthesis are l_{t2}, l_{s2}, l_{f2} and r_{f2}.

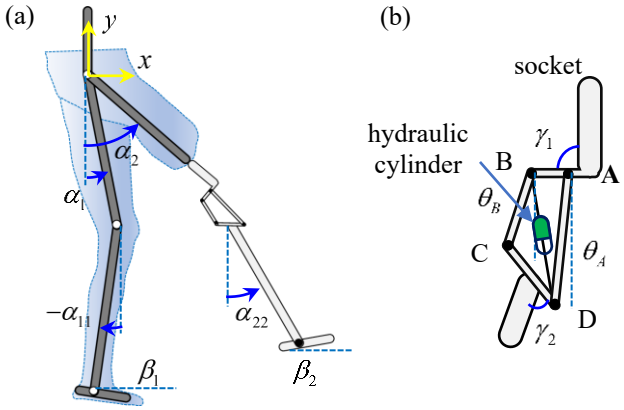

FIGURE 1: The schematic view of the coupled healthy limb and the prosthesis: (a) the multibody system and (b) the four-bar linkage prosthetic knee

2.1. Force representation of the foot-ground contact

For ease of modelling, this paper assumes that the foot only contacts the ground at the toe and the heel. Therefore, the normal pressure to the ground can be represented by the Kelvin-Voigt model, which is given by

$$F_{N,i} = \frac{1}{2}\left(K_{N,i} y_{foot,i} + \chi_{N,i}\dot{y}_{foot,i}\right)\left(1-\mathrm{sgn}\left(y_{foot,i}\right)\right), \quad (1)$$

where $F_{N,i}$ indicates the normal pressure, $K_{N,i}$ means the contact stiffness, $\chi_{N,i}$ represents the contact damping, $y_{foot,i}$ means the vertical position of the foot, and i denotes the contact point of toe or heel. Assume that the dry friction coefficient between the foot and the ground is μ, the friction force caused by the normal pressure can be represented by the Coulomb friction model

$$F_{f,i} = -\mu F_{N,i}\,\mathrm{sgn}\left(\dot{x}_{foot,i}\right) \quad (2)$$

where $F_{f,i}$ is the friction force and $\dot{x}_{foot,i}$ indicates the relative velocity between the foot and the ground.

Note that the contact forces defined by Eqs. (1) and (2) are non-smooth, the gait analysis of the established model will be very difficult. Therefore, we introduce the arctan function to smooth these two equations

$$F_{N,i} = \left[\frac{1}{2} - \frac{\arctan\left(C_1 y_{foot,i}\right)}{\pi}\right]\left(K_{N,i} y_{foot,i} + \chi_{N,i}\dot{y}_{foot,i}\right) \tag{3}$$

$$F_{f,i} = -\frac{2\arctan\left(C_2 \dot{x}_{foot,i}\right)}{\pi}\mu F_{N,i} \tag{4}$$

where C_1 and C_2 are constants and represent the intensity of the smoothness.

2.2. Motion representation of the passive prosthesis

The passive prosthesis consists of the four-bar linkage prosthetic knee, of which the physical parameters are given in TABLE 1. The motion of the linkages in the prosthetic knee follows the constrain condition

$$\overrightarrow{AB} + \overrightarrow{BC} + \overrightarrow{CD} + \overrightarrow{DA} = \vec{0} \tag{5}$$

This expression may also be represented in the planar Cartesian coordinates as

$$\begin{cases} \xi_1 := l_{AB}\sin\left(\gamma_1 + \alpha_1\right) + l_{AD}\sin\theta_A - l_{BC}\sin\theta_B \\ \quad - l_{CD}\sin\left(\gamma_2 + \alpha_{11}\right) = 0 \\ \xi_2 := l_{AB}\cos\left(\gamma_1 + \alpha_1\right) + l_{AD}\cos\theta_A - l_{BC}\cos\theta_B \\ \quad - l_{CD}\cos\left(\gamma_2 + \alpha_{11}\right) = 0 \end{cases} \tag{6}$$

where l_{AB}, l_{AD}, l_{BC}, and l_{CD} are the lengths of the linkages AB, AD, BC, and CD.

TABLE 1: Physical parameters of the four-bar linkage prosthetic knee

Linkage	**Length** (mm)	**Mass** (g)	**R-inertia** (g.mm^2)
AD	167.0	244.4	852553
BC	78.0	135.6	118791
AB	22.5	333.0	145079
CD	99.2	196.7	340507

As can be seen in FIGURE 1(b), the hydraulic cylinder provides the damping force and the restoring force to coordinate the swing of the prosthesis. Suppose that the coefficients of the damping and the stiffness are k and c, the coordination force provided by the hydraulic cylinder can be represented as

$$F' = -k\left(l - l_0\right) - c\dot{l} \tag{7}$$

where F' is the coordination force, l is the length of the cylinder, $l_0 = 168.79$ mm is the original length. According to the principle of virtual work, the torque generated by the coordination force is

$$\tau_1 = \frac{F' l_{AD} l_{AB}\sin\theta_1}{\sqrt{{l_{AD}}^2 + {l_{AB}}^2 - 2 l_{AD} l_{AB}\cos\theta_1}} \tag{8}$$

where $\theta_1 = 0.5\pi - \alpha_1 + \theta_A$.

By letting $\mathbf{q} = \left(x, y, \alpha_2, \alpha_{22}, \theta_A, \theta_B, \beta_2\right)^T$, the motion of the prosthesis can be represented by the Lagrange equations of the first kind

$$\mathbf{M}(\mathbf{q})\ddot{\mathbf{q}} + \mathbf{C}(\mathbf{q},\dot{\mathbf{q}})\dot{\mathbf{q}} + \mathbf{N}(\mathbf{q}) = \mathbf{F}_{ns}(\mathbf{q}) + \mathbf{F}_s(\mathbf{q}) + \mathbf{\Phi}^T\boldsymbol{\lambda} \tag{9}$$

where $\mathbf{M}(\mathbf{q}) \in \mathbb{R}^{7\times7}$ is the mass matrix, $\mathbf{C}(\mathbf{q},\dot{\mathbf{q}}) \in \mathbb{R}^{7\times7}$ is the Coriolis matrix, $\mathbf{N}(\mathbf{q}) \in \mathbb{R}^{7\times1}$ indicates the effect of gravity, $\mathbf{F}_{ns} \in \mathbb{R}^{7\times1}$ is the vector of non-smooth forces that represent the rotation limit and the foot-ground contact given by Eqs. (3) and (4), $\mathbf{F}_s(\mathbf{q}) \in \mathbb{R}^{7\times1}$ denotes the vector of smooth forces that consists of the coordination torque given by Eq. (8), $\boldsymbol{\lambda}$ is the Lagrange multiplier and $\mathbf{\Phi}$ can be written as

$$\mathbf{\Phi} = \frac{\partial\boldsymbol{\xi}(\mathbf{q})}{\partial\mathbf{q}^{\mathbf{T}}} = \frac{\partial\left(\xi_1,\ \xi_2\right)^T}{\partial\mathbf{q}^{\mathbf{T}}} \tag{10}$$

2.3. Motion representation of the healthy limb

By letting $\mathbf{r} = \left(x, y, \alpha_1, \alpha_2, \alpha_{11}, \beta_1\right)^T$, the motion of the healthy limb may also be represented by the Lagrange equations of the first kind

$$\mathbf{M}(\mathbf{r})\mathbf{r} + \mathbf{C}(\mathbf{r},\dot{\mathbf{r}})\mathbf{r} + \mathbf{N}(\mathbf{r}) = \mathbf{F}_{ns}(\mathbf{r}) + \mathbf{F}_s(\mathbf{r}) \tag{11}$$

where the matrices $\mathbf{M}(\mathbf{r})$, $\mathbf{C}(\mathbf{r},\dot{\mathbf{r}})$, $\mathbf{N}(\mathbf{r})$, and the vector $\mathbf{F}_{ns}(\mathbf{r})$ denote the same physical meanings as explained in Eq. (9). However, the generalized force $\mathbf{F}_s(\mathbf{r})$ is distinct from $\mathbf{F}_s(\mathbf{q})$. In this equation, $\mathbf{F}_s(\mathbf{r}) = \left(0, 0, \tau_{hip,1}, \tau_{hip,2}, \tau_{knee}, \tau_{ankle}\right)^T$ means the bionic torques generated by the CPG. By referring [3], the representations of torques are given as

$$\tau_j = -k_j\left(\theta_j - \tilde{\theta}_j\right) - c_j\dot{\theta}_j \tag{12}$$

where j indicates "*hip,1*", "*hip,2*", "*knee*", and "*ankle*", θ_j represents the relative rotation angles of the joint, k_j and $\tilde{\theta}_j$ are the adaptive stiffness and the reference trajectory defined by the Matsuoka oscillator. The detailed expression of k_j and $\tilde{\theta}_j$ are

$$\begin{aligned} \dot{u}_i^s &= \frac{1}{\tau_i^s}\left(c_i^s u^s - u_i^s + \sum_{j,j\neq i} w_{ij}^s\left(k_j + d_{ij}^s k_i\right) - \beta^s v_i^s + F_{eed,i}^s\left(\mathbf{r},\dot{\mathbf{r}}\right)\right) \\ v_i^s &= \frac{1}{\tau_i^{s\prime}}\left(-v_i^s + k_i\right) \\ k_i &= \max\left(0, u_i^s\right) \end{aligned} \tag{13}$$

$$\begin{aligned} \dot{u}_i &= \frac{1}{\tau_i}\left(c_i u^e - u_i + \sum_{j,j\neq i} w_{ij}\left(\tilde{\theta}_j + d_{ij}\tilde{\theta}_i\right) - \beta v_i + F_{eed,i}\left(\mathbf{r},\dot{\mathbf{r}}\right)\right) \\ v_i &= \frac{1}{\tau_i'}\left(-v_i + \tilde{\theta}_i\right) \end{aligned} \tag{14}$$

$$\tilde{\theta}_i = \begin{cases} \pi/2, u_i > \pi/2 \\ u_i, -\pi/2 \le u_i \le \pi/2 \\ -\pi/2, u_i < -\pi/2 \end{cases}$$

where w_{ij} and w_{ij}^s denote the weights of coupling between different joints, d_{ij} and d_{ij}^s represent the gain of the driving-point feedback, τ_s and τ_i^s determine the period of the oscillation, u^e and u^s are the inputs that trigger the limit-cycle oscillation.

2.4. Heterogeneous model of the coupled system

This paper assumes that the connection between the stump and the socket is rigid. Therefore, the variables x, y, and α_2 shown in $\mathbf{q}$ should be identical with those shown in $\mathbf{r}$. This feature indicates that the prosthesis, modelled by Eq. (9), couples with the healthy limb, modelled by Eq. (11), through the motion of the hip joint. The heterogeneous model of the coupled system can be written as

$$\begin{cases} \mathbf{M}(\mathbf{q})\ddot{\mathbf{q}} + \mathbf{C}(\mathbf{q},\dot{\mathbf{q}})\dot{\mathbf{q}} + \mathbf{N}(\mathbf{q}) = \mathbf{F}_{ns}(\mathbf{q}) + \mathbf{F}_s(\mathbf{q}) + \boldsymbol{\Phi}^T\boldsymbol{\lambda} \\ \mathbf{M}(\mathbf{r})\mathbf{r} + \mathbf{C}(\mathbf{r},\dot{\mathbf{r}})\mathbf{r} + \mathbf{N}(\mathbf{r}) = \mathbf{F}_{ns}(\mathbf{r}) + \mathbf{F}_s(\mathbf{r}) \end{cases}$$

$$s.t. \begin{cases} q_1 = r_1 \\ q_2 = r_2 \\ q_3 = r_4 \end{cases} \quad (15)$$

3. PRELIMINARY ANALYSIS

Eq. (15) gives the heterogeneous model of the coupled healthy limb and prosthesis. It needs to be qualified by the model validation.

3.1. Gait test of level walking

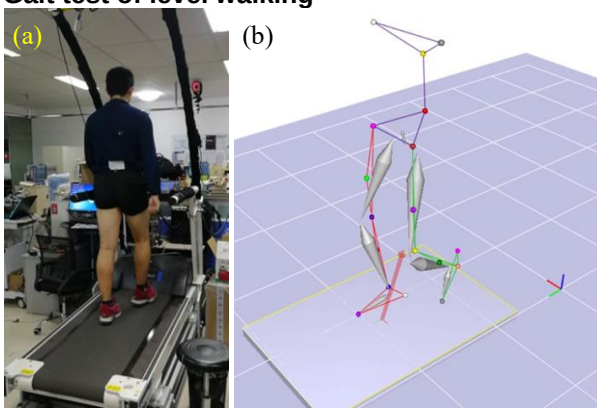

FIGURE 2: Gait test of level walking: (a) photo of the experiment and (b) skeleton view captured by the Motion Analysis system

This paper uses the data measured from a real gait test to qualify the established model. Considering the risk of treadmill walking, an able-bodied testee is chosen rather than the amputee. The gait test has been approved by the Local Ethics Committee of Peking University. As shown in FIGURE 2(a), the treadmill was set to level and running at a constant speed of 1 m/s. 18 markers were stuck on the testee based on the rule of Helen-Hayes. The motion capture instrument, shown in FIGURE 2(b), extracted the motions of the markers at the sampling rate of 100 Hz. To get a sample of steady gait, the test continued for 4 minutes and the motions during the middle 3 minutes were measured.

The measured data are truncated and averaged 30 times for noise removal. The rotation of the trunk is found to maintain tiny during level walking. This feature validates the assumption that the trunk is rigid and stays vertical. FIGURE 3 further gives the motion of the hip joint in one gait period. As can be seen in the plot of $y(t)$, the amplitude of hip lifting is about 3 cm. It is demonstrated later that this variable is a key factor to determine the prosthesis motion.

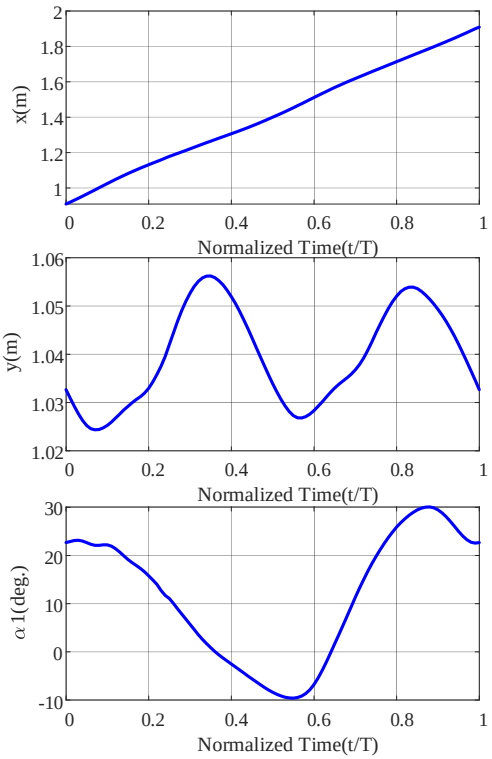

FIGURE 3: The motion of the hip joint in one gait period

3.2. Gait evaluation of the prosthesis

The model given by Eq. (15) is heterogeneous. To simplify the process of model validation, this paper first evaluates the part of the prosthesis. As can be seen in FIGURE 1(a), the prosthesis is driven by the motion of the hip joint. By substituting the measure data, shown in FIGURE 3, into Eq. (9), the motion of the prosthesis can be obtained by numerical simulation. The parameters that represent the foot-ground contact and the intensity of smooth are given in TABLE 2.

TABLE 2: Parameter settings of the foot-ground contact model and the intensity of smooth

Parameter	Setting	Parameter	Setting
K_N	1e5 N/m	C_1	1e6
χ_N	20 Ns/m	C_2	1e4
μ	0.6		

By setting the stiffness and damping of the hydraulic cylinder as $k = 20400$ N/m and $c/k = 0.05$, the time history of the prosthesis's knee angle is calculated. FIGURE 4 shows a comparison between the calculated knee angle and the measured data, where the red solid line represents the former and the blue dashed line indicates the latter. It is obvious that the model of the prosthesis mimics the gait of the testee well.

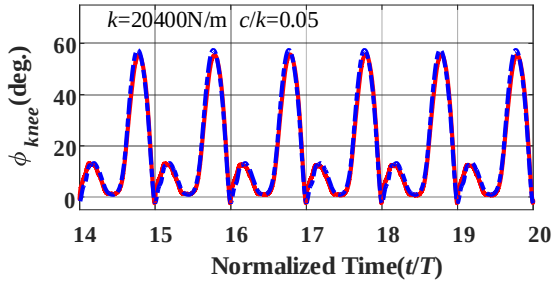

FIGURE 4: Comparison between the calculated knee angle (red solid line) and the measured data (blue dashed line)

By decreasing the stiffness of the hydraulic cylinder, an interesting phenomenon is observed. As can be seen in FIGURE 5, the prosthesis yields a strongly nonlinear response called the period-doubling. When the stiffness is set as $k = 14000$ N/m, the period of the prosthesis motion is double of that of the testee. When the stiffness is set $k = 15200$ N/m, the period becomes three times of that of the testee. This phenomenon is probably caused by the unilateral force representation, a strongly nonlinear model, of the foot-ground contact effect.

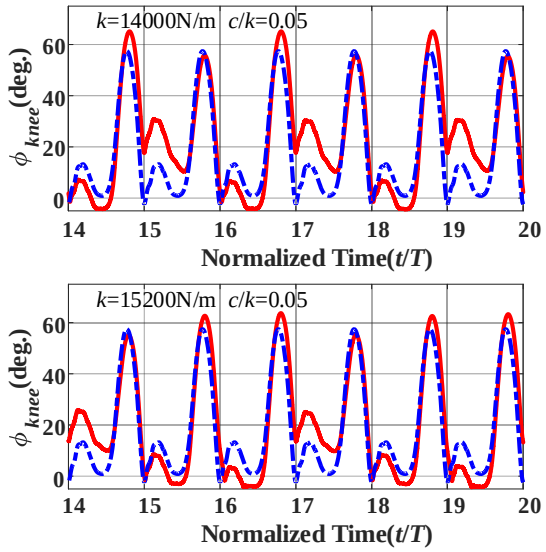

FIGURE 5: Phenomenon of period-doubling

Further numerical studies find that if the amplitude of the vertical motion of the hip joint is amplified a bit, the period-doubling gait will return to the single-period pattern. FIGURE 6 shows the motion of the prosthesis with the same parameter settings except that the amplitude of the vertical motion of the hip joint, namely y, is amplified by 6%. This dynamic bifurcation, which mimics the process of hip swing adaption, provides new insight into the compensatory mechanism for lamely walking.

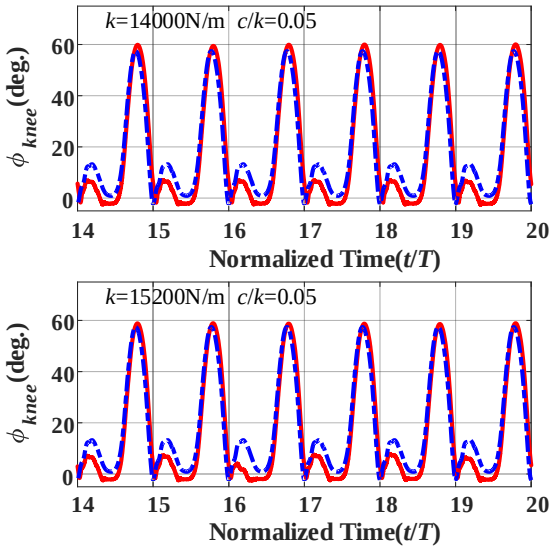

FIGURE 6: Single-period pattern of the prosthesis motion

3.3. Gait simulation of the heterogeneous model

The isolated model of the prosthesis has been validated based on a real gait test. A further step is taken to simulate the gait of the amputee based on the heterogeneous model. The parameters of the CPG are set the same as those in [3]. The snapshots of a single gait process are shown in FIGURE 7. As can be seen, the heterogeneous model can mimic the gait of the amputee.

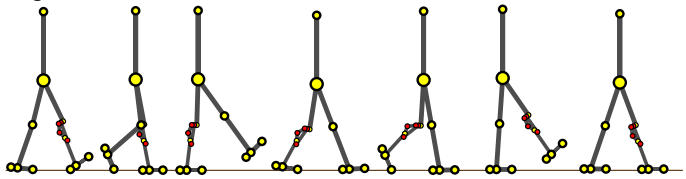

FIGURE 7: Snapshots of a single gait process

However, it is still too early to conclude that the heterogeneous model is perfect. In the numerical simulation, a lot of parameters need to be tried to get a piece of the steady motion. The coupling between the prosthesis and the healthy limb makes the model more unstable. A stability analysis should be further made.

First, the fixed point should be found from the periodic solution of the gait. A Poincare Map that helps find the fixed point can be defined as [25]:

$$P: G \to G$$
$$G = \left\{ \boldsymbol{\psi} \mid y_{heel}\left(\mathbf{q}\right) = 0 \right\} \tag{16}$$

Theoretically, walking gaits correspond to solutions $\boldsymbol{\psi}(t)=\left(\mathbf{q}(t)\quad \mathbf{r}(t)\quad \dot{\mathbf{q}}(t)\quad \dot{\mathbf{r}}(t)\right)^T$ of the heterogeneous model that are periodic, i.e., $\boldsymbol{\psi}(t)=\boldsymbol{\psi}(t+T)$ for a minimum period T and all t. These solutions define isolated orbits in state-space known as *limit cycles*, which correspond to equilibria of the return map $P: G \to G$. This map P represents the system as a discrete system between impact events G, which occur when the heel of the prosthesis impacts on the ground, and sends $\boldsymbol{\psi}_j \in G$ ahead one step to $\boldsymbol{\psi}_{j+1}=P(\boldsymbol{\psi}_j)$ (the subscript j indicates the jth walking step of the gait). The solution $\boldsymbol{\psi}(t)$ is supposed to have a fixed point $\boldsymbol{\psi}^*=P(\boldsymbol{\psi}^*)$.

Taking the fact that the Poincare Map define in Eq. (16) is strongly nonlinear, this paper adopts the Particle Swarm Optimization Algorithm (PSO) [26] to find the fixed point. The PSO is an intelligent algorithm inspired by the foraging behavior of birds. In the PSO algorithm, the speed and the position of the particles are updated according to the cost function of each particle or group. The cost function is defined at the beginning of our algorithm:

$$f=\left|P(\boldsymbol{\psi})-\boldsymbol{\psi}\right|_1 \tag{17}$$

Our optimization objective is to find the minimum of f. When f reaches its minimum value, $P(\boldsymbol{\psi})-\boldsymbol{\psi}$ is supposed to be smallest so that the fixed point $\boldsymbol{\psi}^*$ is found.

Due to the constraints of the ground, the actual number of independent states is only 10. So, each particle is a 10-dimensional vector $\boldsymbol{\eta}$. A group of the PSO consists of 30 particles.

$$\begin{aligned}\boldsymbol{\eta}=(&\alpha_1 \quad \alpha_2 \quad \alpha_1-\alpha_{11} \quad \alpha_2-\alpha_{22} \quad \beta_1\\ &\dot{\alpha}_1 \quad \dot{\alpha}_2 \quad \dot{\alpha}_1-\dot{\alpha}_{11} \quad \dot{\alpha}_2-\dot{\alpha}_{22} \quad \dot{\beta}_1)^T\end{aligned} \tag{18}$$

The searching range of each parameter is determined as follows:

$$\begin{aligned}\alpha_1&:(-20\sim-10)\pi/180 rad & \dot{\alpha}_1&:-1\sim 2 rad/s\\ \alpha_2&:(20\sim 30)\pi/180 rad & \dot{\alpha}_2&:-3\sim 0 rad/s\\ \alpha_1-\alpha_{11}&:(0\sim 10)\pi/180 rad & \dot{\alpha}_1-\dot{\alpha}_{11}&:0\sim 1 rad/s\\ \alpha_2-\alpha_{22}&:(0\sim 10)\pi/180 rad & \dot{\alpha}_2-\dot{\alpha}_{22}&:0\sim 1 rad/s\\ \beta_1&:(-10\sim 0)\pi/180 rad & \dot{\beta}_1&:-1\sim 0 rad/s\end{aligned}$$

Other state variables can be obtained according to the ground constraints：

$$\begin{aligned}x&=-l_{f1}(1-r_{f1})\cos\beta_1-l_{s1}\sin\alpha_{11}-l_{t1}\sin\alpha_1\\ y&=-l_{f1}(1-r_{f1})\sin\beta_1+l_{s1}\cos\alpha_{11}+l_{t1}\cos\alpha_1\\ \beta_2&=\arcsin\left[\left(y-l_{t2}\cos\alpha_2-l_{s2}\cos\alpha_{22}\right)/\left(l_{f2}r_{f2}\right)\right]\\ \dot{x}&=\dot{\beta}_1 l_{f1}(1-r_{f1})\sin\beta_1-\dot{\alpha}_{11}l_{s1}\cos\alpha_{11}-\dot{\alpha}_1 l_{t1}\cos\alpha_1\\ \dot{y}&=-\dot{\beta}_1 l_{f1}(1-r_{f1})\cos\beta_1-\dot{\alpha}_{11}l_{s1}\sin\alpha_{11}-\dot{\alpha}_1 l_{t1}\sin\alpha_1\\ \dot{\beta}_2&=\left(\dot{y}+\dot{\alpha}_2 l_{t2}\sin\alpha_2+\dot{\alpha}_{22}l_{s2}\sin\alpha_{22}\right)/\left(l_{f2}r_{f2}\cos\beta_2\right)\end{aligned}$$

θ_A, θ_B and $\dot{\theta}_A, \dot{\theta}_B$ can be calculated using Eq. (6). Thus $\boldsymbol{\psi}$ is obtained by $\boldsymbol{\eta}$ and constraints.

In the process of parameter iteration, the optimal parameter of particle i in previous iterations is recorded as $\mathbf{p}_i$, and the optimal parameter of all particles in previous iterations is recorded as $\mathbf{g}$. The rule for parameter updating is defined as follows:

$$\begin{aligned}\mathbf{v}_i&=w\mathbf{v}_i+c_1r_1(\mathbf{p}_i-\boldsymbol{\eta}_i)+c_2r_2(\mathbf{g}-\boldsymbol{\eta}_i)\\ \boldsymbol{\eta}_i&=\boldsymbol{\eta}_i+\mathbf{v}_i\end{aligned} \tag{19}$$

where w is the inertia coefficient, c_1 and c_2 are the learning coefficients, r_1 and r_2 are random numbers between 0 and 1. The subscript i indicates the ith particle.

30 iterations are conducted to get the optimal particle $\mathbf{g}$, then $\boldsymbol{\psi}^*$ is obtained by $\mathbf{g}$ and the constraints. The stability of the gait at the fixed point $\boldsymbol{\psi}^*$ is analyzed by using the Jacobian matrix at the fixed point, which is defined as:

$$\mathbf{J}=\left(P(\boldsymbol{\psi}^*+\Delta\boldsymbol{\psi})-P(\boldsymbol{\psi}^*)\right)/\Delta\boldsymbol{\psi} \tag{20}$$

where $\Delta\boldsymbol{\psi}$ is a small perturbation (1e-5 for $\mathbf{q}$ and $\mathbf{r}$, 1e-4 for $\dot{\mathbf{q}}$ and $\dot{\mathbf{r}}$). If the moduli of all the eigenvalues are smaller than 1, the fixed point is stable.

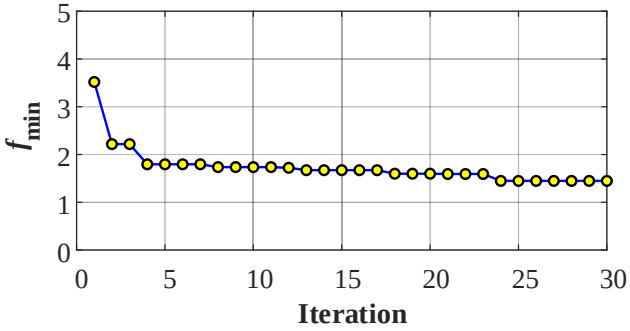

FIGURE 8: Variation of the minimum cost function value

Following the method above, the optimal particle $\mathbf{g}$ is obtained:

$$\begin{aligned}\mathbf{g}=(&-0.2201 \quad 0.3805 \quad 0.0211 \quad 0.0388 \quad -0.0120\\ &-0.1344 \quad -1.9049 \quad 0.6274 \quad 0.6219 \quad 0.1438)^T\end{aligned}$$

And the cost function $f_{\min}=1.448$. The variation of the minimum cost function value is shown in FIGURE 8. Theoretically, if the optimal particle is the fixed point of the periodic orbit, the cost function should be ideally zero. The minimum value achieved here, i.e. $f_{\min}=1.448$, indicates that the gait control signal cannot guarantee the stability of the system. This is because the heterogeneous model built in this paper is a new model, whereas the CPG model is referred from [3] without any modification. By calculating the Jacobian matrix at the fixed point, the maximum moduli of the eigenvalues is 5.94. In the simulation with the optimal parameters, the model falls after 5 strides, which is much more stable than that without

stability optimization. This feature indicates the importance of stability optimization in gait control. Meanwhile, the CPG model that governs the gait should be further modified to fit heterogeneous model.

4. CONCLUSION

This paper provided a heterogeneous dynamic model for gait analysis of the amputee with the passive prosthesis. The representation of the effect of foot-ground contact was refined and the CPG was introduced in the motion control of the healthy limb. A gait test was carried out to validate the model. Preliminary analysis showed that the proposed model mimics the gait of the amputee well. It should also be highlighted that because of the way of foot-ground contact modelling, this paper found a new standpoint to explain the mechanism for lamely walking.

Further studies can be made to complete the heterogeneous model. This paper has not achieved a stable and continuous gait on the proposed model. This is because the driving signal is generated by strictly referring the CPG model in [3]. Note that the constraint conditions and the system itself are modified, experiments should be carried out for a more accurate estimation of the parameters of the foot-ground contact and the CPG. The nonlinear dynamic analysis may also be employed to figure out the feature of the stability of the system.

ACKNOWLEDGMENTS

This research is supported by the National Key Research and Development Project of China (Grant No. 2018YFB1307305) and the National Natural Science Foundation of China (Grant No. 11902077).

REFERENCES

[1] D. J. Braun, J. E. Mitchell, and M. Goldfarb, "Actuated dynamic walking in a seven-link biped robot," IEEE/ASME Trans. Mechatronics, vol. 17, no. 1, pp. 147-156, 2012.

[2] R. D. Gregg, T. Lenzi, L. J. Hargrove, and J. W. Sensinger, "Virtual constraint control of a powered prosthetic leg: From simulation to experiments with transfemoral amputees," IEEE Trans. Robot., vol. 30, no. 6, pp. 1455-1471, 2014.

[3] Y. Huang and Q. N. Wang, "Torque-stiffness-controlled dynamic walking: Analysis of the behaviors of bipeds with both adaptable joint torque and joint stiffness," IEEE Robot. Autom. Mag., vol. 23, no. 1, pp. 71-82, 2016.

[4] A. S. Carvalho and J. M. Martins, "Exact restitution and generalizations for the Hunt–Crossley contact model," Mech. Mach. Theory, vol. 139, pp. 174-194, 2019.

[5] B. Li, S. M. Wang, V. Makis, and X. Z. Xue, "Dynamic characteristics of planar linear array deployable structure based on scissor-like element with differently located revolute clearance joints," P. I. Mech. Eng. C-J Mec., vol. 232, no. 10, pp. 1759-1777, 2018.

[6] W. Goldsmith and J. T. Frasier, "Impact: The Theory and Physical Behavior of Colliding Solids," J Appl. Mech.-T ASME, vol. 28, no. 4, pp. 639, 1961.

[7] N. Mostaghel and D. Todd, "Representations of Coulomb friction for dynamic analysis," Earthq. Eng. Struct. D., vol. 26, no. 5, pp. 541-548, 1997.

[8] L. Liu and Z. Wu, "A new identification method of the Stribeck friction model based on limit cycles," P. I. Mech. Eng. C-J Mec., vol. 228, no. 15, pp. 2678-2683, 2014.

[9] E. Kamenar and S. Zelenika, "Nanometric positioning accuracy in the presence of presliding and sliding friction: Modelling, identification and compensation," Mech. Based Des. Struc., vol. 45, no. 1, pp. 111-126, 2017.

[10] K. Johanastrom and C. Canudas-De-Wit, "Revisiting the LuGre friction model," IEEE Contr. Syst. Mag., vol. 28, no. 6, pp.101-114, 2008.

[11] H. Wang, Y. Sun, and Y. Tian, "Mechanical Structure Design and Robust Adaptive Integral Backstepping Cooperative Control of a New Lower Back Exoskeleton," Stud. Inform. Control, vol. 28, no. 2, pp. 133-146, 2019.

[12] F. Ikhouane, V. Mañosa, and G. Pujol, "Minor loops of the Dahl and LuGre models," Appl. Math. Model., vol. 77, pp. 1679-1690, 2020.

[13] T. Tjahjowidodo, F. Al-Bender, H. V. Brussel H V, and W. Symens, "Friction characterization and compensation in electro-mechanical systems," J Sound Vib., vol. 308, no. 3-5, pp. 632-646, 2007.

[14] Y. H. Sun, T. Chen, C. Q. Wu, and C. Shafai, "A comprehensive experimental setup for identification of friction model parameters," Mech. Mach. Theory, vol. 100, pp.338-357, 2016.

[15] X. Zhang, J. Xu, and J. Ji, "Modelling and tuning for a time-delayed vibration absorber with friction," J Sound Vib., vol. 424, pp. 137-157, 2018.

[16] D. Quintero, A. E. Martin, and R. D. Gregg, "Toward Unified Control of a Powered Prosthetic Leg: A Simulation Study," IEEE Trans. Control Syst. Technol., vol. 26, no. 1, pp. 305-312, 2018.

[17] M. R. Dimitrijevic, Y. Gerasimenko, and M. M. Pinter, "Evidence for a spinal central pattern generator in humans," Ann. Ny. Acad. Sci., vol. 860, no. 1, pp.360-376, 1998.

[18] L. Righetti and A. J. Ijspeert, "Programmable central pattern generators: an application to biped locomotion control," 2006 IEEE International Conference on Robotics and Automation (ICRA). IEEE, 2006.

[19] N. Van der Noot, A. J. Ijspeert, and R. Ronsse, "Biped gait controller for large speed variations, combining reflexes and a central pattern generator in a neuromuscular model," 2015 IEEE International Conference on Robotics and Automation (ICRA). IEEE, 2015.

[20] G. Morantes, J. Cappelleto, G. Fernandez, et al, "Comparison of CPG topologies for bipedal gait," 2016 IEEE Ecuador Technical Chapters Meeting, 2016.

[21] S. Y. Chong, H. Wagner, and A. Wulf, "Neural oscillators triggered by loading and hip orientation can generate

activation patterns at the ankle during walking in humans," Med. Biol. Eng. Comput., vol. 50, no. 9, pp. 917-923, 2012.
[22] H. Xie, L. Guo, Y. Liu, and F. Li, "The design and modeling of multi-axis knee artificial leg," J. Bioact. Compat. Pol., vol. 24, pp.183-195, 2009.
[23] A. Hamon and Y. Aoustin, "Cross four-bar linkage for the knees of a planar bipedal robot," 10th IEEE-RAS International Conference on Humanoid Robots. IEEE, 2010.
[24] L. Xu, D. H. Wang, Q. Fu, G. Yuan, and L. Z. Hu, "A novel four-bar linkage prosthetic knee based on magnetorheological effect: principle, structure, simulation and control," Smart Mater. Struct., vol. 25, no. 11, pp. 115007, 2016.
[25] Gregg ,R. D. "On the Mechanics of Functional Asymmetry in Bipedal Walking.", IEEE Transactions on Biomedical Engineering, vol. 59, no. 5, pp. 1310-1318, 2012.
[26] Kim, Jeong Jung , J. W. Lee , and J. J. Lee . "Central pattern generator parameter search for a biped walking robot using nonparametric estimation based Particle Swarm Optimization." International Journal of Control Automation & Systems, vol. 7, no. 3, pp. 447-457, 2009.